Electric potential on a WCLL TBM mock-up in MHD experiments as indication for flow distribution in breeder units

L. Bühler *, C. Courtessole, C. Koehly, B. Lyu, C. Mistrangelo

Karlsruhe Institute of Technology (KIT), P.O. Box 3640, 76021 Karlsruhe, Germany

Keywords:
Magnetohydrodynamics (MHD)
Liquid metal breeder blankets
WCLL TBM for ITER
MHD experiments in a scaled mock-up
Electric potential measurements

A B S T R A C T

The distribution of electric potential on the surface of a scaled mock-up of the water-cooled lead lithium test blanket module for ITER has been measured in magnetohydrodynamic experiments using the MEKKA facility at the Karlsruhe Institute of Technology (KIT). The electric potential is a physical quantity that can be recorded with high accuracy. For strong magnetic fields, i.e. for high Hartmann numbers, the potential may be considered as approximate hydrodynamic stream-function of the liquid metal flow, from which the core velocity is obtained by differentiation. Moreover, experimental potential data may be directly compared with numerical simulations for both validation of computational tools and interpretation of measurements. Experimental and numerical data of potential confirm anticipations from measured pressure values that the major fraction of the flow in breeder units occurs near both ends of the module, while in a larger central domain the flow is almost negligible.

1. Introduction

In the water-cooled lead lithium (WCLL) test blanket module (TBM) for of the International Thermonuclear Experimental Reactor (ITER), PbLi is employed as neutron multiplier, breeder material, and heat transfer fluid. The flow of this liquid alloy interacts with the strong plasma-confining magnetic field inducing electric currents that, in turn, generate dominant electromagnetic Lorentz forces responsible for large pressure drop and peculiar velocity distributions. Flow-induced electric currents may leak across common electrically conducting walls between neighboring fluid regions, which leads to electromagnetic coupling of geometrically separated domains.

The design of the WCLL TBM for ITER is shown Fig. 1. The original CAD file was provided to the authors though F4E [1] and it corresponds to the design shown in [2]. The TBM consists of two columns with 2×8 breeder units filled with liquid PbLi. The heat is removed by water-cooling of walls and cooling pipes immersed in the liquid metal. The liquid metal is circulated to ancillary systems for tritium extraction via a set of feeding and draining poloidal manifolds. The purge flow in the breeder units is established by connections to the feeding manifold, radial flow towards the first wall, radial–poloidal–radial turn around the baffle plate, and radial back flow into the draining manifold. The coordinates x, y, z used in the present work are shown in the figure and they correspond to poloidal, toroidal and radial directions as foreseen in ITER.

In recent experiments performed in the MEKKA facility at KIT, magnetohydrodynamic flows have been investigated in a scaled mock-up [3] of the WCLL TBM (see Fig. 2). Those experiments covered a wide range of fusion-relevant parameters in terms of flow rates and strengths of magnetic field. Pressure measurements in the mock-up indicate significant flow imbalance among the breeder units caused by the geometry of the manifolds, which distribute and collect the liquid metal [4,5].

During the experimental campaign, in addition to pressure values, the flow-induced electric potential was recorded by a large number of electrodes installed on the Hartmann wall (the wall perpendicular to the toroidal magnetic field) in the middle of the breeder units. Given that the electric potential is closely related to the liquid metal flow in the module, it serves as an indication of local flow rates. Therefore, potential distributions may be used to quantify flow partitioning among breeder units to confirm previous observations derived from pressure measurements. Moreover, electric potential, which can be measured with high accuracy, may be directly compared with results from numerical simulations for code validation purposes.

2. Experimental setup

In order to support the ITER WCLL TBM development, a scaled (1:2.5) mock-up has been designed and manufactured at KIT [3]. The

* Corresponding author.
E-mail address: leo.buehler@kit.edu (L. Bühler).

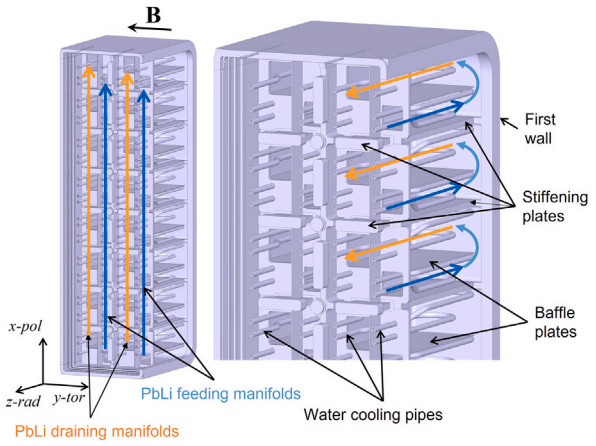

Fig. 1. Original CAD design of the WCLL TBM geometry as provided by CEA. View on internal details such as liquid metal manifolds, water pipes, breeder units, baffle plates and stiffening plates.

MHD mock-up is derived from the original CAD files provided by Fusion for Energy (F4E) [1,2]. As shown in Fig. 2, it consists of one column of 8 breeder units (BUs) stacked along the poloidal direction, feeding (blue) and draining (red) manifolds separated by a baffle wall and connected to the BUs via openings in the back plate. Dummy cylinders mimic water-cooled pipes, representing solid obstacles for the flow. Fig. 2 (middle) displays typical flow paths that involve flow in the feeding manifold (blue), flow in BUs from the back-plate towards the first wall (other colors), turn around the BU baffle plate, backward flow into the draining manifold (red) and further downstream towards the exit pipe. The 3D view (top) displays an insulating plate mounted on the top Hartmann wall, carrying a large number of potential-sensing spring-loaded electrodes.

The distribution of potential on the Hartmann wall at $y = 0$ is of particular interest for assessing the flow partitioning in the BUs. Along the poloidal x-coordinate we have 20 electrodes for each BU, i.e. a total number of 160 pins along the entire poloidal length. As individual potential-sensing electrodes we use spring contact pins, i.e. gold-plated CuBe needles, that are mounted in gold-plated phosphor bronze shafts and pressed to the surface by silver-coated stainless steel springs. The shafts are finally inserted in gold-plated sockets to which the wiring is soldered. Details of the pins are shown in Fig. 3. Before the sensors were mounted to the wall, the surface of the mock-up has been thoroughly cleaned with hydrochloric acid to remove residual oxide layers in order to eliminate contact resistance.

The fully instrumented test section is displayed in Fig. 4. The cables are connected to a multiplexer that switches signals in packages of 15 to a multi-channel nano-voltmeter. The mock-up is installed in the liquid metal loop of the MEKKA facility at KIT (surrogate fluid NaK, inventory 200l, pump 9 bar, 25 m^3/h, possibility for using up to 30 pressure taps, 600 potential sensors, 2.1T magnetic field, uniform with deviations smaller than 1% in a volume of $800 \times 483 \times 168$ mm^3 [6]). The physical properties of NaK, with higher values of the ratio (σ/ρ) compared to PbLi, allow approaching with the available magnetic fields in the laboratory large values of Ha and N (see Section 3) that are relevant for fusion applications.

3. Magnetohydrodynamics scales

For small magnetic Reynolds numbers the magnetic flux density **B** remains unaffected by the liquid metal flow and given by the externally applied magnetic field [7], the magnitude of which is B_0. As an example, for a typical case considered in the present work ($Re = 1000$), the magnetic Reynolds number is $R_m = \mu\sigma u_M L_M = 0.02$ for magnetic

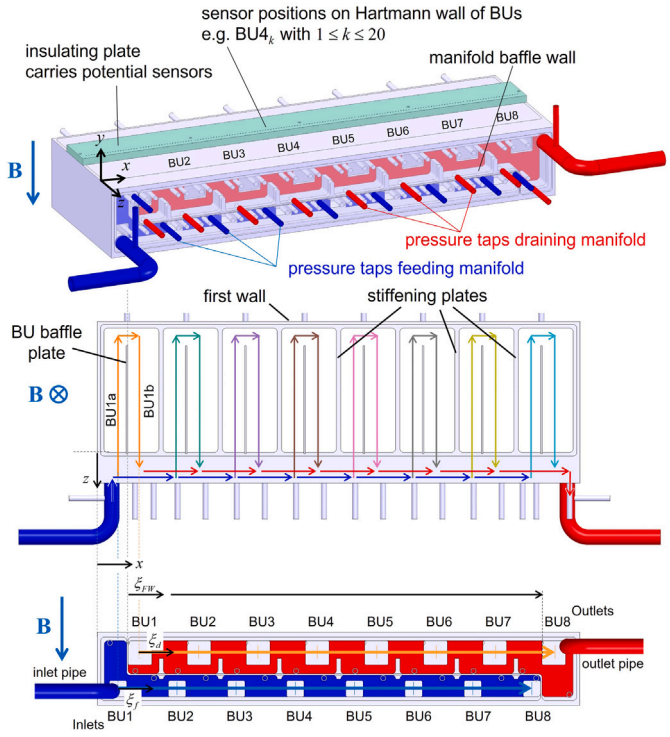

Fig. 2. 3D view (partly transparent) on the mock-up showing positions and nomenclature of potential sensors on the wall (top). Sketch of typical flow paths in manifolds and breeder units in a poloidal–radial x–z slice. BUs are separated from each other by stiffening plates; the flow in BUs is guides by a BU baffle plate (middle). Definition of coordinates x or ξ, which are used for plotting results of potential along the Hartmann wall or pressure along manifolds and first wall, respectively (bottom).

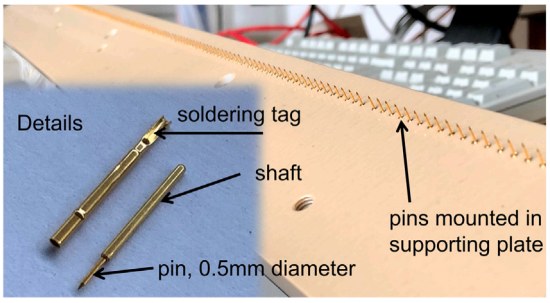

Fig. 3. Details of spring contact pins used in the experiment for sensing wall potential.

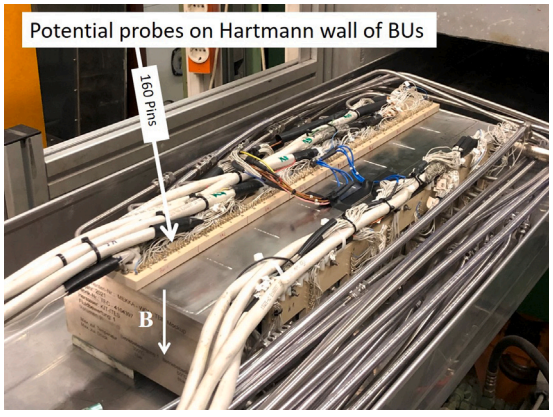

Fig. 4. Test section in front of the magnet with potential sensors installed on the surface of the mock-up. 160 pins on the top Hartmann wall which is perpendicular to the applied magnetic field.

permeability μ and conductivity σ of the model fluid NaK and for velocity $u_M = 0.3$ m/s and length $L_M = 0.0195$ m in manifolds where highest velocities are present.

The electric current density **j** induced by the flow is defined through Ohm's law

$$\mathbf{j} = \sigma\,(-\nabla\phi + \mathbf{u}\times\mathbf{B}) \tag{1}$$

proportional to the specific electrical conductivity σ of the liquid metal and driven by the gradient of the electric potential ϕ and by a flow-induced electric field when the fluid moves with velocity **u**. With a typical length scale L and magnitude of velocity u_0 it is obvious that a reasonable scale for potential in BUs becomes $\phi_0 = u_0 B_0 L$, where the Hartmann length $L = 0.039$ m stands for half of the internal toroidal (y) size of BUs and u_0 represents the assumed mean velocity in one BU, $u_0 = Q/(\rho\, 8 A_{BU}/2)$. Here, the mass density of the fluid is ρ and the total mass flow rate Q is distributed ideally over 8 BUs of cross section A_{BU}. The factor 2 results from the fact that in a single BU the flow is guided by a baffle plate radially to the first wall and then backward towards the back plate so that the efficient average cross section per BU is $A_{BU}/2$.

For strong magnetic fields, as present in liquid metal blankets of a fusion reactor or in the TBM of ITER, the dominant balance of forces acting on the liquid metal core flow establishes between the pressure force and the electromagnetic Lorentz force, i.e. $\nabla p = \mathbf{j}\times\mathbf{B}$. Inertia effects are often negligible and viscous effects are confined to very thin boundary or internal layers. A typical scale for pressure in the manifold is $p_M = \sigma u_M L_M B_0^2$. Here the characteristic velocity scale is defined as $u_M = Q/(\rho A_M)$, where A_M stands for the average cross section of the manifold (feeding plus draining parts). Moreover, the mean Hartmann length in the manifold is only half of that in a BU, since a thin baffle wall divides the cross-section A_M in two parts, i.e. $L_M = L/2$.

The liquid metal flow in BUs is characterized by the Hartmann number and the Reynolds number

$$Ha = LB_0\sqrt{\frac{\sigma}{\rho\nu}} \text{ and } Re = \frac{u_0 L}{\nu}, \tag{2}$$

as nondimensional measures for the strength of magnetic field and velocity, respectively. Here ν stands for the kinematic viscosity of the liquid metal. The interaction parameter that quantifies the ratio of electromagnetic to inertia forces is given as $N = Ha^2/Re$. For applications in PbLi blankets, $N \approx 1.4\times10^3 \div 1.8\times10^5$ and $Ha \approx 6.5\times10^3 \div 3.0\times10^4$ [8]. Both parameters are quite large, which emphasizes the dominance of the Lorentz force and confirms the introduced scaling.

4. Results

Measurements of pressure distribution along the mock-up have been reported in previous publications e.g. in [4,5]. One of those results for $Ha = 1040$ and $Re = 1040$ is shown in Fig. 5 with the purpose of explaining major phenomena that are important for the understanding of potential data discussed later in the present work. The figure shows the variation of pressure along feeding (blue) and draining (red) manifolds with respect to poloidal coordinates ξ that have their origin in the center of windows in the back plate that connect the manifolds with the first BU (for definition of coordinates see Fig. 2). This representation has been chosen since it allows direct identification of pressure heads Δp_{BU} driving the flows in individual BUs. It can be observed that Δp_{BU1} and Δp_{BU8} are significantly larger than pressure heads in the other BUs. As a consequence, we may anticipate that BU1 and BU8 receive more flow than BU2÷BU7. This is caused by the fact, that a large fraction of flow swaps via BU1 (and some via BU2) from the smaller feeding to the larger draining manifold. The flow across BU3÷BU6 is quite small and the flow remaining in the feeding manifold is transferred via BU7 and BU8 into the draining duct. This leads to a flow imbalance between central and outer BUs, and a non-symmetric distribution along the poloidal direction is caused by different cross-sections of feeding

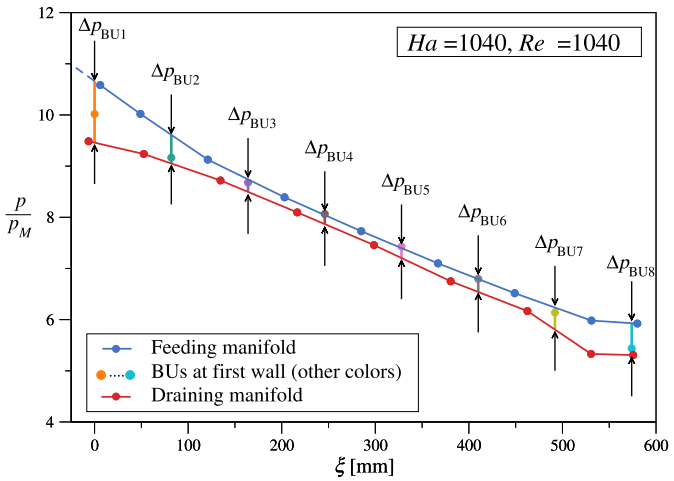

Fig. 5. Measured pressure distribution along feeding (blue) and draining (red) manifolds and at the first wall in BUs (other colors) for $Ha = 1040$, $Re = 1040$. For definition of coordinates or used colors see Fig. 2.

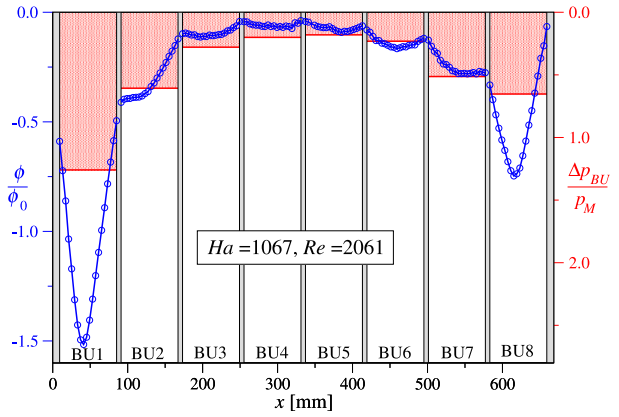

Fig. 6. Distribution of measured potential on the Hartmann wall (blue symbols) for $Ha = 1067$ and $Re = 2061$. For comparison, the pressure heads Δp_{BU} driving flows in BUs are overlain in red.

and draining ducts. Similar results have been predicted by theoretical analyses [9,10] and numerical simulations [11]. Those results are supported in the present work by measurements of electric potential on the Hartmann wall of BUs along the poloidal direction.

The electric potential ϕ is an important flow property since it can be measured with high accuracy and directly compared with numerical simulations. Moreover, it is a good indication of flow pattern since often it may be interpreted as hydrodynamic stream function for the core flow. For instance if duct walls were thin, the major balance in Ohm's law (1) establishes between the induced electric field $\mathbf{u}\times\mathbf{B}$ and the potential gradient,

$$u_z B_0 = \underbrace{\frac{\partial\phi}{\partial x}}_{\gg} + \underbrace{\frac{j_x}{\sigma}}$$

because the last term is often negligible since $|j_x/\sigma| \ll |\partial\phi/\partial x|$.

Some examples of potential measurements along the Hartmann wall of BUs are displayed through Figs. 6÷10 for different Hartmann numbers. The figures reveal that highest values of potential ϕ and potential gradient $\partial\phi/\partial x$ establish in BU1 and BU8, i.e. at the beginning and at the end of the module. In their neighborhood, in BU2 and BU7, the values are already considerably smaller but still higher than in the remaining BU3÷BU6. This observation prevails for all parameters investigated experimentally.

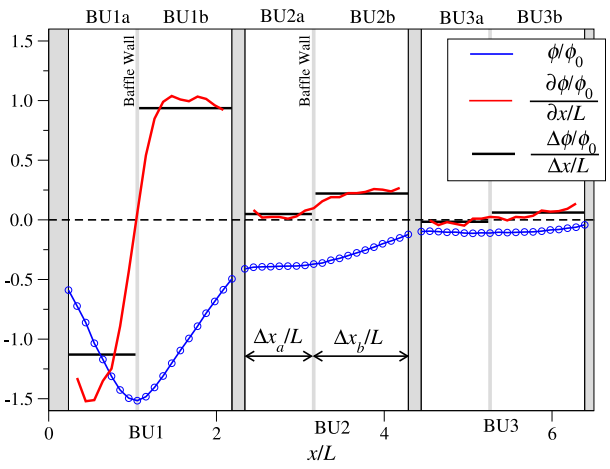

Fig. 7. Distribution of measured potential on the Hartmann wall for $Ha = 1067$ and $Re = 2061$; zoom into the data of Fig. 6. The nondimensional potential gradient (red) denotes approximate radial core velocity and scaled potential differences between walls (black) indicate average velocity in parts of BUs.

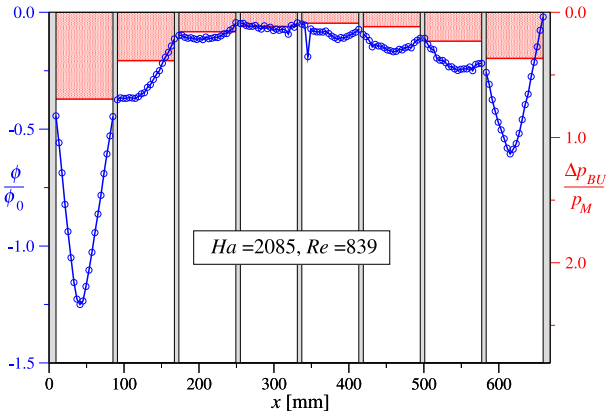

Fig. 8. Distribution of measured potential on the Hartmann wall (blue symbols) for $Ha = 2085$ and $Re = 839$. For comparison, the pressure heads Δp_{BU} driving flows in BUs are overlain in red.

Scaled potential gradients may be interpreted as nondimensional radial core velocity u_z/u_0, or potential differences as flow rates (or mean core velocity $\overline{u_z}/u_0$ when divided by corresponding $\Delta x/L$), i.e.

$$\frac{u_z}{u_0} \approx \frac{\partial\phi/\phi_0}{\partial x/L}, \quad \frac{\overline{u_z}}{u_0} \approx \frac{\Delta\phi/\phi_0}{\Delta x/L}. \tag{3}$$

One result for $Ha = 1067$ and $Re = 2061$ is shown in a detailed view in Fig. 7, which displays the scaled potential gradient as approximate radial (in z direction) core velocity (red lines) according to Eq. (3). The potential differences between stiffening plates and baffle walls approximate the mean core velocity when divided by corresponding $\Delta x/L$ (black lines). We may conclude that there is the strongest radial core velocity towards the first wall in the first compartment BU1a and backwards in BU1b after the flow passed the BU baffle plate near the first wall. There remains some flow in BU2 and the core flow in BU3 is almost zero. Not visible from the Hartmann walls are the high-velocity jets that develop along walls aligned with the magnetic field as predicted in numerical simulations [11]. Those jets are responsible for a significant fraction of flow (about 2/3 of flow in BU1 according to numerical simulations) and they are strongly coupled across common conducting walls. As a result of this electromagnetic coupling, the jets on both sides of a wall are of similar magnitude but with opposite direction [12]. This is the case especially at the BU baffle plates but also at the stiffening plates that separate individual BUs. For instance,

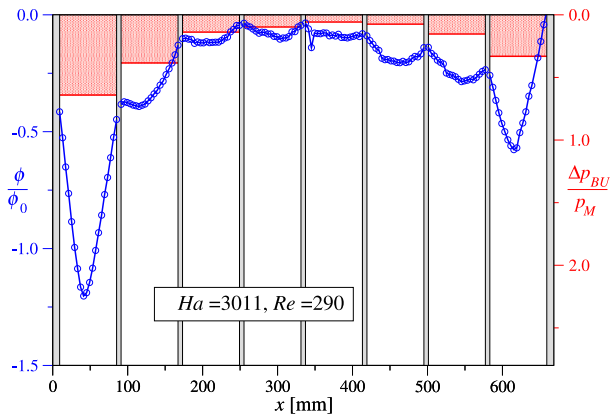

Fig. 9. Distribution of measured potential on the Hartmann wall (blue symbols) for $Ha = 3011$ and $Re = 290$. For comparison, the pressure heads Δp_{BU} driving flows in BUs are overlain in red.

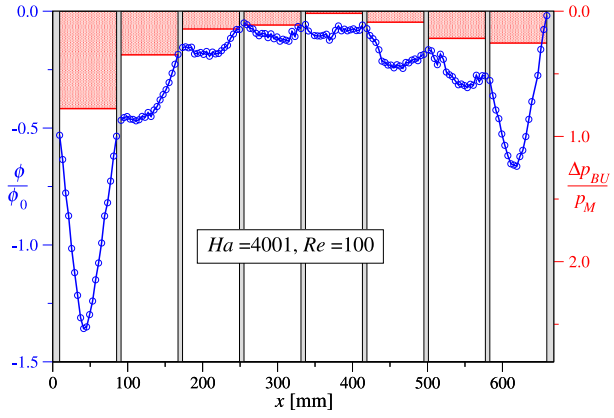

Fig. 10. Distribution of measured potential on the Hartmann wall (blue symbols) for $Ha = 4001$ and $Re = 100$. For comparison, the pressure heads Δp_{BU} driving flows in BUs are overlain in red.

along the stiffening plate between BU1 and BU2 a strong backward jet is present in BU1b that drives by electromagnetic coupling a forward one of comparable strength in BU2a. The latter carries in BU2 nearly all flow towards the first wall while the core velocity in BU2a is almost zero. The fluid is later transferred back mainly in the core of BU2b. In BU3 the velocity appears negligible. Finally, it is worth mentioning that the interpretation of potential data on the outer surface of Hartmann walls as approximate core velocity works best for applications where the walls are thin. In these cases, the potential in the fluid equals the one on the wall and it is constant along magnetic field lines. Therefore, core velocity is constant along **B** as well. For thicker walls, as in the present case of the TBM, one should be aware that estimates of velocity on the basis of surface potential data may lose some precision.

As outlined above, the distribution of potential provides insight on core velocity and flow partitioning. Those results may be compared with the driving pressure heads along BUs. Fig. 6 displays for comparison the pressure heads Δp_{BU1}.....Δp_{BU8} driving the flow through BU1 ..... BU8, respectively (red). Those pressure heads are obtained experimentally from measured pressure data along manifolds, interpolated to the centers of entrance and exit windows in the back plate (see Fig. 5). A comparison of pressure and potential data supports the evidence that the major fraction of the flow is carried in BUs near the ends of the module, whereas the flow in BU3÷BU6 is insignificant. This has been confirmed for all parameters investigated here experimentally as displayed in Figs. 8÷10 (see Fig. 9).

Non-uniform flow partitioning among BUs is also confirmed by numerical simulations of MHD flow in an entire column of BUs based on

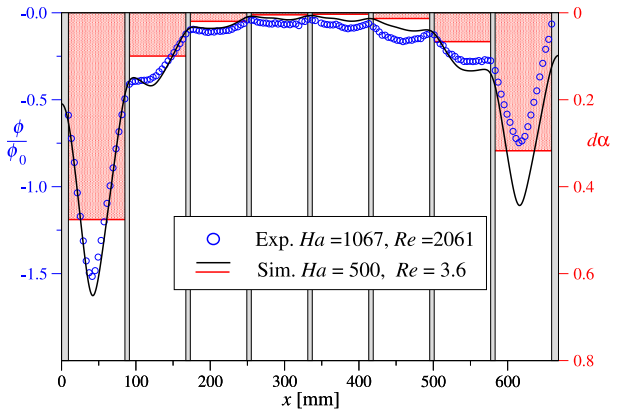

Fig. 11. Distribution of potential on the Hartmann wall of BUs. Comparison of experimental data (blue symbols) and numerical simulation (solid line). Theoretical results for flow rate fractions $d\alpha = Q_{BU}/Q$ in BUs are overlain in red.

the CAD model of the MHD mock-up [3]. A comparison of nondimensional electric potential obtained from measurements and calculations, as displayed in Fig. 11, shows quite good agreement confirming both the quality of the numerical work and the accuracy of experimental data. Indeed, the modeling of the flow in an entire mock-up is quite challenging since all geometrical details have been numerically resolved, including thin MHD boundary layers along all walls and the walls themselves, requiring a grid with more than 160 million cells. Even with such an enormous discretization effort, the highest value of the Hartmann number reached so far in calculations was limited to $Ha = 500$. However, such a value appears already large enough that results are close to an asymptotic regime, where properly scaled flow quantities approach finite values independent of Ha. A comparison with measurements for $Ha = 1000$ confirms this expectation. We observe a very good agreement for the scaled potential distribution along almost the entire poloidal direction. Some discrepancy may be observed in BU8, the reason of which is still under investigation. Nevertheless, the comparison provides high confidence in the simulation results. The latter, which yield detailed velocity profiles, have been used to determine the fractions $d\alpha = Q_{BU}/Q$ of flow carried by individual BUs. Those results are superimposed on Fig. 11 for comparison with potential distribution. We observe that about half of the total flow (48%) is exchanged between the manifolds via BU1 and about 10% via BU2. The flow through BU3÷BU6 is quite small. The rest of the flow is transferred from the feeding to the draining manifold via BU7 (6.6%) and BU8 (31.7%). As a result, the numerically determined flow imbalance is in agreement with data shown in Fig. 7 and even more expressed than the one expected from measurements of BU pressure heads Δp_{BU}.

5. Conclusions

Measurements of electric potential distribution along the Hartmann wall of 8 BUs have been performed for MHD flows in a scaled mock-up of the ITER TBM. For strong magnetic fields, i.e. for high Hartmann numbers, the experimental data may be interpreted in terms of approximate core velocity or local flow rates in individual BUs. The measured data for scaled potential compares well with numerical simulations so that we may use the latter to determine theoretically the flow distribution and to get a more detailed picture of the velocity profiles in the blanket module. Results confirm previous expectations based on pressure measurements [5] that the flow is non-uniformly distributed among BUs with almost no flow in BU3÷BU6. This fact demands a design revision of the manifolds in order to achieve a more uniform flow partitioning that is better suited for tritium extraction [10].

CRediT authorship contribution statement

L. Bühler: Writing – review & editing, Writing – original draft, Visualization, Validation, Investigation, Formal analysis, Data curation, Conceptualization. **C. Courtessole:** Writing – review & editing, Writing – original draft, Visualization, Methodology, Investigation, Formal analysis, Data curation, Conceptualization. **C. Koehly:** Visualization, Investigation. **B. Lyu:** Validation, Investigation, Formal analysis, Data curation. **C. Mistrangelo:** Writing – review & editing, Writing – original draft, Validation, Investigation, Formal analysis, Data curation, Conceptualization.

Declaration of competing interest

The authors declare that they have no known competing financial interests or personal relationships that could have appeared to influence the work reported in this paper.

Acknowledgments

This work has been carried out within the framework of the EUROfusion Consortium, funded by the European Union via the Euratom Research and Training Programme (Grant Agreement No 101052200 — EUROfusion). Views and opinions expressed are however those of the author(s) only and do not necessarily reflect those of the European Union or the European Commission. Neither the European Union nor the European Commission can be held responsible for them.

Data availability

Data will be made available on request.

References

[1] T. Batal, Assembly of WCLL TBM: CAD product and parts (by CEA), personal communication, EUROfusion IDM reference: EFDA-D-2M9E39 V1.1 - PMI-7.1.1 Task 2-T004-D001 Deliverable D5: Draft version of System Description Document chapters related to Design description of the WCLL TBM set, 2019.

[2] J. Aubert, G. Aiello, D. Alonso, T. Batal, R. Boullon, S. Burles, B. Cantone, F. Cismondi, A. Del Nevo, L. Maqueda, A. Morin, E. Rodríguez, F. Rueda, M. Soldaini, J. Vallory, Design and preliminary analyses of the new Water Cooled Lithium Lead TBM for ITER, Fusion Eng. Des. 160 (2020) 111921, http://dx.doi.org/10.1016/j.fusengdes.2020.111921.

[3] C. Koehly, L. Bühler, C. Courtessole, Design of a scaled mock-up of the WCLL TBM for MHD experiments in liquid metal manifolds and breeder units, Fusion Eng. Des. 192 (2023) 113753, http://dx.doi.org/10.1016/j.fusengdes.2023.113753.

[4] C. Courtessole, H.-J. Brinkmann, L. Bühler, J. Roth, Experimental investigation of MHD flows in a WCLL TBM mock-up, Fusion Eng. Des. 202 (2024) 114306, http://dx.doi.org/10.1016/j.fusengdes.2024.114306.

[5] C. Courtessole, H.-J. Brinkmann, L. Bühler, J. Roth, Characterization of MHD pressure losses in a mock-up of the WCLL test blanket module, Fusion Eng. Des. accepted (2025).

[6] L. Barleon, K.-J. Mack, R. Stieglitz, The MEKKA-Facility a Flexible Tool To Investigate MHD-Flow Phenomena, Tech. Rep. FZKA 5821, Forschungszentrum Karlsruhe, 1996, http://dx.doi.org/10.5445/IR/270039825.

[7] R. Moreau, Magnetohydrodynamics, Kluwer Academic Publisher, 1990.

[8] M. Abdou, N.B. Morley, S. Smolentsev, A. Ying, S. Malang, A. Rowcliffe, M. Ulrickson, Blanket/first wall challenges and required R & D on the pathway to DEMO, Fusion Eng. Des. 100 (2015) 2–43, http://dx.doi.org/10.1016/j.fusengdes.2015.07.021.

[9] L. Bühler, C. Mistrangelo, A simple MHD model for coupling poloidal manifolds to breeder units in liquid metal blankets, Fusion Eng. Des. 191 (2023) 113552, http://dx.doi.org/10.1016/j.fusengdes.2023.113552.

[10] L. Bühler, C. Mistrangelo, Geometric optimization of electrically coupled liquid metal manifolds for WCLL blankets, IEEE Trans. Plasma Sci. 202 (2024) 114306, http://dx.doi.org/10.1109/TPS.2024.3362689.

[11] C. Mistrangelo, L. Bühler, V. Klüber, Towards the simulation of MHD flow in an entire WCLL blanket mock-up, Fusion Eng. Des. 193 (2023) 113752, http://dx.doi.org/10.1016/j.fusengdes.2023.113752.

[12] S. Molokov, Fully developed liquid-metal flow in multiple rectangular ducts in a strong uniform magnetic field, Eur. J. Mech. B Fluids 12 (6) (1993) 769–787.